Proceedings of GT2007
ASME Turbo Expo 2007: Power for Land, Sea and Air
May 14-17, 2007, Montreal, Canada

GT2007-27434

Computational Analysis of Surface Curvature Effect on Mist Film Cooling Performance

Xianchang Li
Department of Mechanical Engineering
Lamar University
Beaumont, TX 77710

Ting Wang
Energy Conversion & Conservation Center
University of New Orleans
New Orleans, LA 70148-2220

ABSTRACT

Air film cooling has been widely employed to cool gas turbine hot components such as combustor liners, combustor transition pieces, turbine vanes and blades. Enhancing air film cooling by injecting mist with tiny water droplets with diameters of 5-10μm has been studied in the past on flat surfaces. This paper focuses on computationally investigating the curvature effect on mist/air film cooling enhancement, specifically for film cooling near the leading edge and on the curved surfaces. Numerical simulations are conducted for both 2-D and 3-D settings at low and high operating conditions. The results show, with a nominal blowing ratio of 1.33, air-only adiabatic film cooling effectiveness on the curved surface is less than on a flat surface. The concave (pressure) surface has a better cooling effectiveness than the convex (suction) surface, and the leading edge film cooling has the lowest performance due to main flow impinging against the coolant injection. By adding 2% (weight) mist, film cooling effectiveness can be enhanced approximately 40% at the leading edge, 60% on the concave surface, and 30% on the convex surface. The leading edge film cooling can be significantly affected by changing of the incident angle due to startup or part-load operation. The film cooling coverage could switch from the suction side to the pressure side and leave the surface of the other part unprotected by the cooling film. Under real gas turbine operating conditions at high temperature, pressure, and velocity, mist cooling enhancement could achieve 20% and provides a wall cooling of approximately 180K.

Keywords: film cooling, surface curvature, mist cooling, heat transfer enhancement

NOMENCLATURE

b	slot width (m)
d	diameter (m)
k	turbulence kinetic energy (m^2/s^2)
M	blowing ratio, $(\rho u)_c/(\rho u)_g$
Re	Reynolds number, ud/ν
s	distance along a surface
T	temperature (K, ^oF)
u	streamwise velocity component (m/s)
v	spanwise velocity component (m/s)
x, y, z	coordinates

Greek Symbols

ε	turbulence dissipation rate (m^2/s^3)
η	adiabatic film cooling effectiveness, $(T_g-T_{aw})/(T_g-T_c)$
ν	kinematic viscosity (m^2/s)
ρ	density (kg/m^3)

Subscript

aw	adiabatic wall
c	coolant or jet flow
g	hot gas/air
0	air-only film cooling

INTRODUCTION

Cooling of gas turbine hot components is a critical task because these components such as combustor liners, combustor transition pieces, turbine vanes (nozzles) and blades (buckets) need to be protected from the flue gas at extremely high temperature. External air film cooling as well as internal cooling has been successfully used in protecting turbine airfoils for the last half-century [1-2] with a continuous research effort striving to make the cooling more effective.

Film cooling --- In film cooling, there are many flow and geometric parameters that affect the cooling performance, such as jet hole shape, coolant injection angle, blowing ratio, inlet velocity profile, turbulence intensity, and coolant-supply plenum configuration, etc. In general, cooling can be optimized with a comprehensive study of the effect of all these factors. For example, Jia et al. [3] investigated a slot jet film cooling by using numerical simulations together with experiments. Kwak and Han [4-5] measured heat transfer coefficients and film-cooling effectiveness on a gas turbine blade tip. Wang et al. [6] conducted an experimental study focusing on the flow mixing behavior inside the slots. Bell et al. [7] studied film cooling from shaped holes and measured the local and spatially averaged adiabatic film cooling effectiveness. Brittingham and Leylek [8] performed numerical simulation on film cooling with compound-angle shaped holes and concluded that superposition of individual effects for compound-angle cylindrical holes and streamwise shaped holes do not necessarily apply to compound-angle shaped holes. A recent study by Colban et al. [9] compared cylindrical and fan-shaped film cooling on a vane endwall at low and high free-stream turbulence levels. Their

results revealed that the film-cooling effectiveness decreased with increasing blowing rate for the cylindrical holes while the fan-shaped passage showed increased film-cooling effectiveness. Suryanarayanan et al. [10] measured film-cooling effectiveness under rotation on the rotor blade platform. It is found that film-cooling effectiveness increases with an increase in the coolant-to-mainstream mass flow ratios for all turbine speeds. Higher turbine rotation speeds show stronger spread of local film cooling effectiveness on the platform.

Curvature effect on film cooling ---Most of these studies used flat surfaces and a supplied main flow. In the real gas turbine application, the film cooling flow in the leading edge area is subject to impingement from the main flow (shower-head cooling), which possesses very different flow mechanism from those further downstream where the main flow is basically parallel to the surface. The coolant flow structure will also be affected by the strong curvature near the leading edge. The strong leading-edge curvature is further demarcated into concave and convex curvature on the suction surface and pressure surface, respectively. There are a number of studies investigating the film cooling flow mechanisms at the leading edge and the effect of surface curvature on cooling effectiveness. Nicolas and Le Meur [11] analyzed the equations governing the equilibrium conditions of a cool gas film injected along a curved wall. Compared to the constant-pressure flat plate, the performance is improved for a concave wall with relatively high mass flow rate ratios; In the case of the convex wall, the cooling efficiency of the film is less than that on a plate with the same streamwise pressure gradient. Mayle et al. [12] studied slot jet film cooling along a flat, convex, and concave surface. Compared to the results for the flat surface, convex curvature is found to increase the adiabatic wall effectiveness whereas concave curvature is found to be detrimental. Mayle et al.'s finding seems to be opposite to the Nicolas and Le Meur's study. Ito et al. [13] measured the local film cooling with a row of jets on a gas turbine blade by a mass transfer technique. The static pressure force around the jet pushed a near tangential jet towards the convex wall, which produced a higher effectiveness than that on a flat wall when the momentum flux ratio was small. At a large momentum flux ratio, the inertia of the jet forced the jet to move away from the wall and the cooling effectiveness became smaller. The effect of curvature on the concave side is the reverse of those for the convex surface. Later, Schwarz et al. [14] showed that the opposite performance might be caused by different coolant injection rates. The effects of injection rate and curvature on the film cooling performance were studied on a convex surface. At low blowing rates, film cooling is more effective on the convex surface than on a flat or a concave surface. As the injection rate is increased, normal and tangential jet momentum promotes liftoff from the convex surface, thereby lower the performance. Jiang and Han [15] studied the effect of film hole row location on local film cooling effectiveness distribution on a turbine blade model. Results indicated that injection from a different film hole row location provides a different effectiveness distribution on pressure and suction surfaces depending on local mainstream velocity and blade curvature. Berhe and Patankar [16] conducted a numerical study to investigate the effect of surface curvature on cooling effectiveness. For the low blowing ratios considered, the convex surface resulted in a higher cooling effectiveness than both the flat and concave surfaces. For the convex case, the coolant jet is pressed to the surface by a strong cross-stream pressure gradient. On the concave surface, the mixing between the coolant jet and the mainstream is strong, so the cooling effectiveness degrades. To enhance the film cooling performance in the vicinity of the turbine blade leading edge, Kim et al. [17] investigated the flow characteristics of the film-cooled turbine blade using a cylindrical body model. The inclination of the cooling holes is along the radius of the cylindrical wall and 20^o relative to the spanwise direction. Their results show that the blowing ratio has a strong effect on film cooling effectiveness as well as the coolant trajectory. The local spanwise-averaged effectiveness can be improved by locating the first-row holes near the second-row holes.

Mist cooling --- As the working gas temperature continuously increases to augment thermal efficiency, new cooling techniques are needed to surpass incremental improvements of convectional gas turbine cooling technologies. A promising technology to enhance film cooling is to inject water mist (small droplet) into the coolant flow. Each droplet acts as a cooling sink and flies over a distance before it completely vaporizes. This "distributed cooling" characteristics allows controlled cooling by manipulating different sizes of injected water droplets. The flow temperature reduces mainly due to droplet evaporation and partially due to larger specific heats of water and water vapor. Another important merit of employing mist film cooling is that some larger droplets can fly longer and evaporate farther into the downstream region where single-phase air film cooling becomes less effective. Li and Wang [18-19] simulated air/mist film cooling and showed that a small amount of mist injection (2% of the coolant mass flow rate) could increase the adiabatic cooling effectiveness about 30%~50% under low temperature, velocity and pressure conditions similar to those in the laboratory. The effects of different flow parameters, injection hole configuration, and coolant supply plenum on the cooling effectiveness were also studied. Under the GT operating conditions with high temperature and high pressures (Wang and Li [20]), the cooling enhancement was found less attractive in terms of "enhancement percentage" (10~20%) than the cases with low pressure, velocity and temperature conditions. However, due to high surface temperature in the real gas turbine condition, relatively smaller percentage of cooling enhancement can result in larger wall temperature reduction, which is critical to significantly extend the life expectancy of gas turbine airfoils. Recently, Li and Wang [21] presented the air/mist film cooling heat transfer coefficient under non-adiabatic wall condition including conjugate condition employing internal channel cooling. Result of conjugated 2-D cases indicated that heat conduction from downstream to upstream along the solid wall is strong. The streamwise heat even conducts back to the film cooling jet flow in the neighborhood of the jet hole within a distance of 5 slot widths.

Enhancing heat transfer by injecting tiny water droplets is not a new concept. Related applications have been developed and research has been conducted. One example is gas turbine inlet cooling [22]. Furthermore, fog overspray is used to provide cooling in the compressor. Petr [23] performed a thermodynamic analysis of the gas turbine cycle with wet compression based on detailed simulation of a two-phase compression process. Nirmalan et al. [24] conducted an experimental study of turbine vane heat transfer with water-air mist cooling. The authors' research group has conducted a series of mist/steam cooling experimental studies by injecting fine droplets into steam flow [25-28] for application in the H-type gas turbine using a closed-loop steam cooling scheme. The highest local heat transfer enhancement of 200% was achieved with 1~5% (weight) mist in a straight pipe flow [25], and the average enhancement was 100%. In a 180^o tube bend [26], the overall cooling enhancement ranged from 40% to 300% with the maximum local cooling enhancement being over 800%, which occurred at about 45^o downstream of the inlet of the test section. For jet impingement cooling over a flat surface [27], a 200% cooling enhancement was obtained near the stagnation point by adding 1.5% mist (in mass). For jet impingement on a concave surface [28], enhancements of 30 to 200% were achieved within five-slot distance with 0.5% (weight) mist.

The previous mist/air film cooling simulations were conducted on flat surfaces with the main flow moving in parallel with the surface [18-21]. This paper will focus on investigating the shower-head film cooling near the leading edge, and the subsequent curved surface effects on mist film cooling. The flow fields over the curved surfaces are expected to create a body force exerted on the water droplet by the cross-stream pressure gradient. It will be interesting to see how these effects would alter the water droplet dynamics and lead to different film cooling performance from that on a flat surface. The simulation is conducted under different settings, including gas turbine operating conditions at high temperatures and pressures.

NUMERICAL MODEL

Airfoil and Cooling Hole Configurations

While the configuration of the internal channel and jet holes in real gas turbine airfoil can be complicated, a simplified schematic of turbine blade with film cooling holes is shown in Fig. 1a. In general, the coolant air enters the cooling channel from the blade root and then is injected through holes at locations of leading edge, side surfaces, and trailing edge. The complete cooling process is a combination of external film cooling and internal convective cooling.

Figure 1b shows the periodic computational domain for 2D cases and the injection holes (slots). The blade has a chord length of 0.215m, and the distance between two blades is 0.225m. There are a total of 30 blades with a hub diameter of 2.15m. The injection angle for both pressure and suction sides is 35^o while the injection angle at the leading edge is 75^o. The size of all the holes is about 1 mm. The jet hole is located at 30 mm downstream from the leading edge on suction side and 20 mm on pressure side. For the 3D case shown in Fig. 1c, the flow is approximated as periodic in the radial direction so that only one of the holes in a row is considered. The hole has a diameter of 1mm. The hole lies in the plane of the main inlet velocity vector and the leading edge with an angle of 55^o to the main flow. The center-to-center distance between two adjacent holes is 10mm.

Numerical Method

To simulate film cooling with mist, it is feasible to consider the droplets as a discrete phase since the volume fraction of the liquid is usually small (< 10%). The droplets are tracked in a Lagrangian frame of reference, and the mass, momentum and heat transfer are computed between the discrete phase and the continuous flow. The effect of droplets on the continuous phase is incorporated as a source term to the governing equations. This method has been used in many studies such as dispersion of post-dryout dispersed flow [29], evaporating droplets in a swirling jet [30], and evaporating spray in turbulent gas flow [31]. The Lagrangian method has also been used in the studies of mist film cooling with a flat surface by the authors [18-21].

To apply the discrete phase model to mist film cooling, the time-averaged, steady-state Navier-Stokes equations as well as equations for mass, energy and species transport are solved. Since the Reynolds number (Re) of the main flow (based on the duct height and the inlet condition) is over 90,000, a turbulence model has to be considered. In this study, the standard k-ε model is employed. Since the standard k-ε model is mainly valid for high Reynolds number fully turbulent flow, an enhanced wall function is used for the region close to the wall. Basically, the whole domain is separated into a viscosity-affected region and a fully turbulent region by defining a turbulent Reynolds number. The standard k-ε model is used in the fully turbulent region, and the one-equation model of Wolfstein [32] is used in the viscosity-affected region. The turbulent viscosities calculated from these two regions are blended to smooth the transition. The constants in turbulence equations are consistent with [33]. More details on the governing equations as well as the turbulence model were documented in [18 and 19] and are not repeated here. An extended discussion on the turbulence model is given later in this paper.

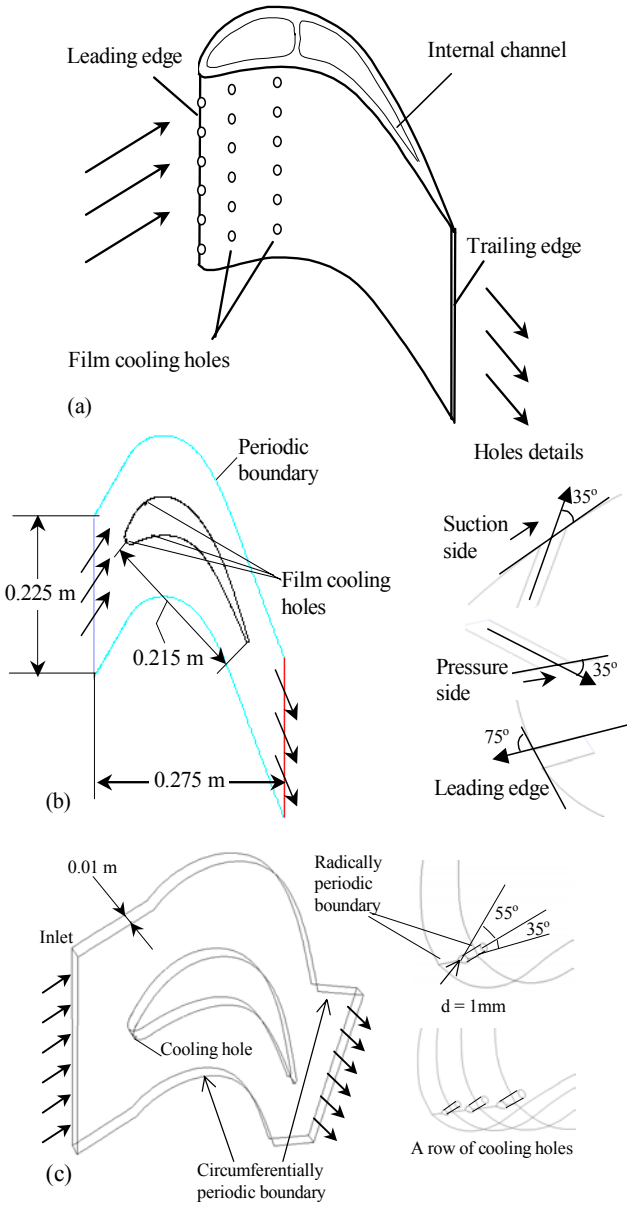

Figure 1 Schematic of film cooling and computational domain (a) film cooling concept (b) 2-D cases (c) 3-D cases

Stochastic Particle Tracking – The standard k-ε turbulence model is based on the time-averaged equations. Using this flow velocity to trace the droplet will result in an averaged trajectory. In the real flow, the instantaneous velocity fluctuation would make the droplet dance around this average track. However, the instantaneous velocity is not calculated in the current approach as the time averaged Navier-Stokes equations are solved. One way to simulate the effect of instantaneous turbulence on droplets dispersion is to use the stochastic tracking scheme [34]. Basically, the droplet trajectories are calculated by using

the instantaneous flow velocity ($\bar{u} + u'$) rather than the average velocity ($\bar{u}$). The velocity fluctuation is then given as:

$$u' = \zeta\left(\overline{u'^2}\right)^{0.5} = \zeta(2k/3)^{0.5} \quad (1)$$

where ζ is a normally distributed random number. This velocity will apply during a characteristic lifetime of the eddy (t_e), given from the turbulence kinetic energy and dissipation rate. After this time period, the instantaneous velocity will be updated with a new ζ value until a full trajectory is obtained. When the stochastic tracking is applied, the basic interaction between droplets and continuous phase keeps the same, accounted by the source terms in the conservation equations. The source terms are not directly but rather indirectly affected by the stochastic method. For example, the drag force between droplets and the airflow depends on the slip velocity calculated by the averaged Navier-Stokes equations if without the stochastic tracking. With the stochastic tracking a random velocity fluctuation is imposed at an instant of time, and the drag force and additional convective heat transfer will be calculated based on this instantaneous slip velocity. The source terms associated with this instantaneous drag force and convective heat transfer enter the momentum and energy equations without any additional formulation. For a steady-state calculation, the "instant of time" means "each iteration step." Therefore, the averaged momentum equation will not be affected by the stochastic tracking scheme; rather the trajectory of the droplet will reflect the effect of the imposed instantaneous perturbation.

Boundary Condition Setup

Airflow – Two sets of operating conditions are considered. The first set is for a typical laboratory condition featured with low temperature, velocity and pressure. The main flow is assumed to be dry air (zero humidity). Uniform velocity (10 m/s) and temperature (400K) are assigned to the mainstream inlet. Coolant flow is assigned as saturated air (100% relative humidity). Jet inlet velocity is 10 m/s, and the temperature is 300K. The blowing ratio, which is defined as $M = (\rho v)_{jet} / (\rho v)_{main}$, is 1.33 in this case. The inlet condition of the turbulence is specified by the turbulence intensity and the hydraulic diameter to calculate the turbulence length scale. The turbulent intensity is 3% at mainstream inlet and 1% at the coolant flow inlet. The flow exit (outlet) of main computational domain is assumed to be at a constant pressure of 1 atm. All the walls in the computational domain are adiabatic and have a no-slip velocity boundary condition. Note that the above assigned temperature and velocity conditions are referenced in several previous studies of air-film cooling, for example [7] and [8].

The second set of parameters is associated with practical gas turbine operating conditions, featured with high temperature, velocity and pressure. The main flow in this case has a temperature of 1561K and a velocity of 128 m/s, while the jet flow has a temperature of 644K and a velocity of 106 m/s. These parameters give a blowing ratio of 2, and a Reynolds number of 1.61×10^6, based on a chord length of 0.215 m. The operational pressure is 15 atm. These settings are not selected to match any specific commercial model but they are a realistic representation of typical gas turbine operating conditions.

Droplet Injection – The droplet is uniformly given as either 5 or 10 μm. The mass ratio of mist over cooling airflow is 2% for lower operating conditions, which is about 7.0×10^{-4} kg/s for the 2-D slot with a width of 1mm and a unit depth of one meter. For the high operating condition, the mist concentration is 10% because more heat needs to be absorbed in this case due to the large temperature difference. Mist is injected at 10 locations uniformly distributed along the 2D jet inlet. The 3D case is run at low operating conditions, and the injection number is 41. The trajectory number for stochastic tracking is chosen to be 25. The boundary condition of droplets at walls is assigned as "reflect", which means the droplets elastically rebound off once reaching the wall. At the outlet, the droplets just simply flee/escape from the computational domain.

Meshing and Simulation Procedures

To conduct numerical simulation, the computational domain is meshed with a proper setup on the boundary conditions. As shown in Fig. 2, unstructured and nonuniform grids are constructed in this study, and the basic element is triangles for the 2D case. The grids near the blade surface as well as the cooling holes are denser than the other areas. Furthermore, the near-wall grid is adapted twice (4 times finer) to capture the wall effect on calculated results for both single-phase and mist film-cooling cases. The total number of the cells for 2D domain is 62,800, while the 3D domain has a total grid of 337,000 (not shown in the figure).

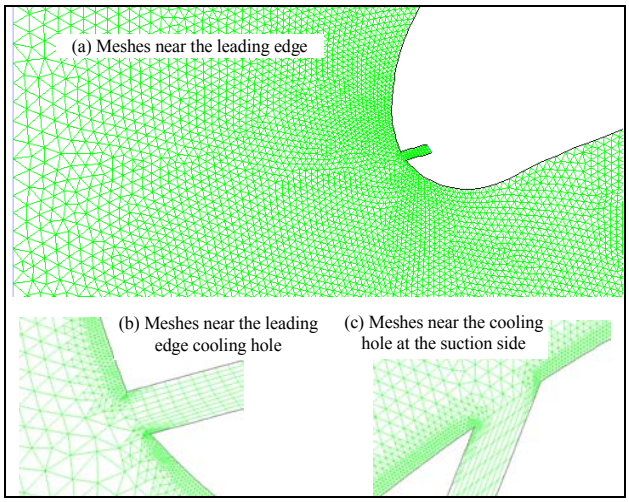

Figure 2 Meshes of partial domain and details near Injection holes (with grid adaptation)

The commercial software package Fluent (version 6.2.16) from Fluent, Inc. is adopted. The simulation uses the segregated solver, which employs an implicit pressure-correction scheme [34]. The SIMPLE algorithm is used to couple the pressure and velocity. Second order upwind scheme is selected for spatial discretization of the convective terms and species. Lagrangian trajectory calculations are employed for the dispersed phase of droplets. After obtaining an approximate flow field of the airflow, the droplet trajectories are calculated. At the same time, drag, heat and mass transfer between the droplets and the airflow is calculated.

Iteration proceeds alternatively between the continuous and discrete phases. Ten iterations in the continuous phase are conducted between two iterations in the discrete phase. Converged results are obtained after the residuals are less than the specified values. A converged result renders mass residual of 10^{-4}, energy residual of 10^{-6}, and momentum and turbulence kinetic energy residuals of 10^{-5}. These residuals are the summation of the imbalance for each cell, scaled by a representative of the flow rate. Typically, 2000 to 4000 iterations are needed to obtain a converged result, which takes about 4~5 hours physical time on a 2.8 GHz Pentium 4 personal computer for a 2D case and 5-10 times longer for the 3D cases.

Discussion of the Modeling

The flow near the leading edge of a turbine blade actually impinges on the surface and creates a strong streamwise pressure gradient near the stagnation region. The high strain rate and anisotropic characteristics in this region require appropriate adjustment of turbulence model. However, the presence of the high-pressure gradient field usually suppresses any turbulence production and could even relaminarize the flow in the boundary layer. Therefore, appropriate handling of laminar-turbulent transition downstream of the leading edge is also important despite the laminar flow in the gas turbine environment being more of "disturbed" nature attributed to high free-stream turbulence and unsteady disturbance. All of these above mentioned phenomena further complicate prediction and modeling of the flow field. In this study, no attempt has been made to tackle the complexity of the above issues.

Note that the constants adopted in the turbulence model may not be the most appropriate values for mist film cooling flow, especially on the flow near the leading edge. Usually these constants need to be "tuned" for different flow physics such as impingement flow, accelerated flow, decelerated flow, separated flow, low-Reynolds number flow, curved flow, and rotating flow, etc. Since a better knowledge is needed on what values these turbulence constants should be for a mist film cooling flow, the current approach is thought to be conservative by not tuning the values of these constants. Furthermore, the main purpose of this study is to investigate the effect of adding mist to the air flow on film cooling effectiveness, rather than study how turbulence models should be modified to predict mist film cooling flow more accurately under the influence of curvature. Therefore, using the same values of these turbulence constants for both the air-only flow and the air/mist flow provides a controlled condition for a meaningful comparison of the results. Again, the detailed turbulence model and associated constants were documented in [18 and 19] and are not repeated here.

RESULTS AND DISCUSSION

1. Film Cooling Near Turbine Blade Leading Edge (2-D Slot)

1.1 Air-only Film Cooling at Low Operating Conditions

Figure 3 shows the velocity vector and temperature distribution close to the leading edge. The inlet velocity for both jet and main flow is 10 m/s and the inlet temperature is 400K for main flow and 300K for jet flow, respectively. The coolant injection is located slightly above the stagnation point of the main flow. Near the leading edge, the main gas flow essentially impinges to the surface. The local hot gas flow has only a small velocity component parallel to the cooling surface and the injection momentum is retarded by the opposing momentum of the impinging main flow. Both phenomena are different from film cooling mechanism over a flat surface. Therefore, the local blowing ratio (or effective blowing ratio) at the leading edge will have a different value although the nominal blowing ratio is 1.33 in this case.

As discussed earlier, the blowing angle at the leading edge is 75° rather than a smaller value (30-35°) optimized for a flat surface due to the specific position of leading edge versus the main flow. There is a relatively strong circulation due to flow separation close to the jet exit, which will generally lower the cooling effectiveness, especially for 3D holes (Li and Wang [18]) due to the strong mixing between the hot flow and the coolant. The temperature profile and adiabatic cooling effectiveness along the cooling surface are given in Fig. 4. Note that s/2b in the figure is the dimensionless distance on the specified surface, and b is the slot width. The result of film cooling with a flat surface is also given for comparison. The adiabatic cooling effectiveness (η) is defined as:

$$\eta = (T_g - T_{aw})/(T_g - T_c) \quad (2)$$

where T_g is the mainstream gas temperature, T_c is the temperature of the coolant (jet), and T_{aw} is the adiabatic wall temperature. The value of η ranges from 0 (no cooling) to 1 (perfect cooling), which usually serves as an indicator to examine the performance of film cooling.

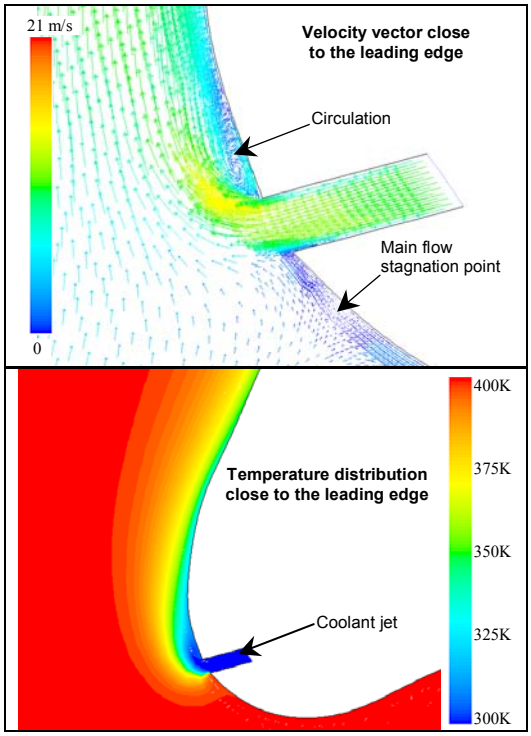

Figure 3 Flow pattern and temperature distribution

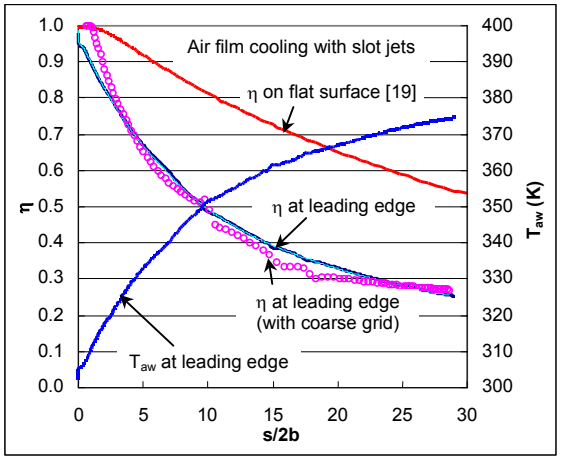

Figure 4 Comparison of air-only leading-edge adiabatic cooling effectiveness with that on a flat surface with the same nominal blowing ratio of 1.33.

Figure 4 shows that on both leading edge and flat surface, the adiabatic cooling effectiveness decreases with the distance away from the injection hole; however, the adiabatic cooling effectiveness is lower near the leading edge than on a flat surface. Besides the difference due to geometry and flow fields, the lower velocity parallel to the wall makes the penetration in the normal direction relatively stronger than that in the tangential direction, especially when the injection angle is big. The effect of surface curvature is another reason for the low cooling effectiveness. Furthermore, the strong circulation close to jet injection results in a higher mixing and lower adiabatic cooling effectiveness immediately downstream of the hole (s/2b<1). On the other hand, different lines for the adiabatic cooling effectiveness in Fig. 4 summarize the grid sensitivity study. When the grid becomes finer (for example, adapted close to the wall), the results collapse to the same curve (2 lines for η at the leading edge), which indicates the independence of simulation results on grid systems.

1.2 Mist Film Cooling at Low Operating Conditions

As seen in previous studies [18-21], injecting mist into the coolant airflow can improve the performance of air film cooling. The tiny water droplets will stay close to the coolant jet and absorb heat via evaporation to keep the coolant temperature low. Figure 5 shows the droplets' trajectories for the case of leading edge cooling. The droplets have a diameter of 5μm in this figure. The droplets roughly follow the coolant streamlines, adhere to the wall area, and quickly vaporize. However, some of the droplets do penetrate through the coolant zone and move into the main flow. This means the strayed droplets lower the temperature of the main flow rather than the coolant flow, which makes the cooling enhancement lower than the case on a flat surface.

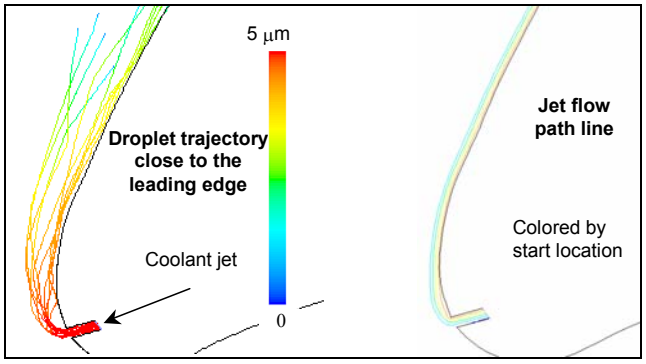

Figure 5 Droplet Trajectories vs. jet flow pathlines for Leading Edge Mist Cooling

Figure 6 gives the cooling effectiveness with 2% mist (by mass) and 5-μm droplet. Compared to air-only film cooling, η increases from 0.28 to 0.38 at s/2b = 25. Also shown in Fig. 6 is the ratio of adiabatic cooling effectiveness with and without mist, η_{mist}/η_0. By defining the enhancement as $[(\eta_{mist}/\eta_0)-1]$, the maximum enhancement can reach 44% at a location downstream from s/2b = 14 to 22. The average cooling enhancement is 25~30%. Comparing the current results with the findings over flat surfaces in [18], the enhancement ratio of mist cooling at the leading edge is higher at s/2b = 5~20, which is partially due to the lower air film cooling at the leading edge (see Fig. 4). The cooling enhancement ratio becomes smaller farther downstream on the concave wall, whereas the enhancement on the flat surface maintains a high value of 44% downstream of s/b = 5. This is caused by the concave surface effect to be discussed in detail later.

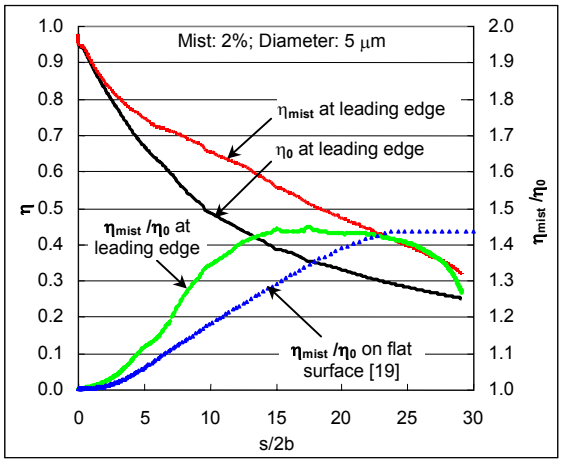

Figure 6 Enhancement of adiabatic cooling effectiveness by injecting mist with the nominal blowing ratio of 1.33

Note that mist film cooling itself can be improved by using different droplet sizes and concentrations. Figure 7 shows the cooling effectiveness and enhancement ratio when different droplet sizes and mist concentration are employed. As expected, larger droplets make the enhancement lower due to their stronger penetration into the main flow and smaller surface to volume ratio, while higher concentration enhances air film cooling more significantly due to more available latent heat. For example, the enhancement at s/2b = 25 increases from 10 to 20% when the mist concentration increases from 2% to 5%. On the other hand, when the droplet size increases from 5 to 10μm, the enhancement becomes small (5% in average). Certainly, in a real application, the droplets will have a distributed size, and the cooling performance will be a combination of the results with different sizes of uniform droplets.

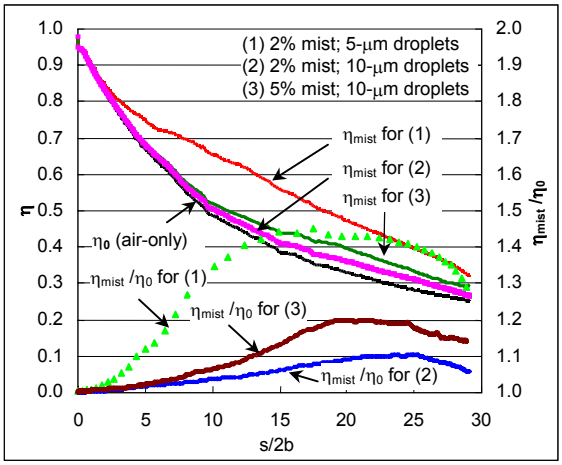

Figure 7 Effects of the droplet size and mist concentration on film cooling enhancement at the leading edge

1.3 Effect of Incident Angle on Cooling of the Leading Edge

In case of startup or partial load, the incident angle of main flow will change. The effect of the incident angle on leading-edge film cooling performance is examined. Figure 8 shows the flow pattern as well as the temperature distribution with a new angle, which is 15° smaller than that in Sections 1.1 and 1.2. The coolant flow is significantly affected by the incident angle. Since the stagnation point

of the main flow moves to a location above the injection hole, most of the coolant flow turns down to the pressure side rather than the suction side as in the previous cases. This movement of stagnation point makes the film protection on the pressure side well but the suction side undesirable. The coolant jet is quickly bent and pushed toward the wall by the incoming main flow; hence the cooling film does not travel too far downstream and results in a quickly degraded cooling effectiveness from 0.8 to 0.3 within a distance of 15 slot widths on the pressure side as shown in Fig. 9. Although some cooling also prevails on the suction side, the cooling effectiveness is lower than 0.3. When mist is injected during the partial load condition, cooling enhancement is observed in both sides with an enhancement of 30~50%.

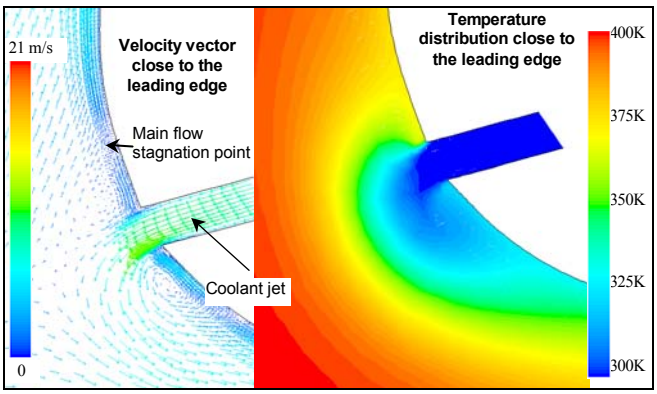

Figure 8 Effect of the main flow incident angle on flow and temperature distribution close to the leading edge

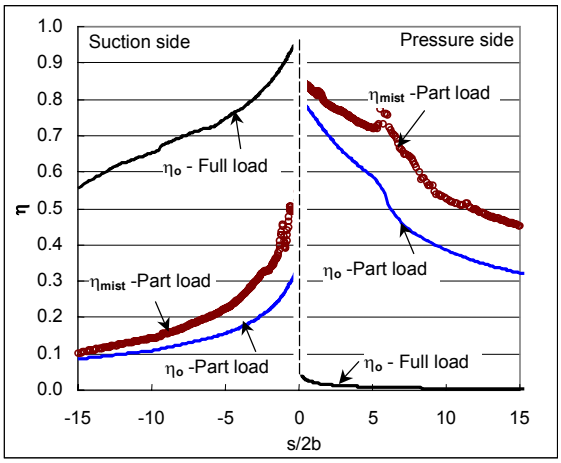

Figure 9 Effect of the main flow incident angle on adiabatic film cooling effectiveness near the leading edge.

1.4 Mist Film Cooling at High Operating Conditions

All the cases in Sections 1.1-1.3 are conducted at low operating conditions to be comparable with other studies in the public literature. These cases can be used to show the fundamental phenomena of film cooling with and without mist injection. However, gas turbines are usually operated at very high pressure, temperature, and velocity. The performance of air film cooling and mist film cooling could be different. To simulate a typical gas turbine operating condition, the main flow has a temperature of 1561K and a velocity of 128 m/s, and the jet flow has a temperature of 644K and a velocity of 106 m/s. These parameters give a blowing ratio of 2 and a Reynolds number of 1.61×10^6 (based on the length scale of 0.215 m). The operating pressure is 15 atm. Figure 10 shows the enhancement is relatively low, even with a high mist concentration (10%). This is because the large temperature difference (T_g-T_j = 1561-644 = 917K) in high operating conditions needs larger wall temperature drop to reach the same unit percentage of cooling effectiveness; whereas this temperature difference is 100K (400-300) under the low temperature and pressure conditions. For example, a 30K wall temperature reduction will contribute to 30 percentage points of η value (based on T_g-T_j = 400-300K) under low pressure and temperature conditions, whereas the same 30K wall temperature reduction will only harness 3.3 percentage of η enhancement under elevated GT operating conditions. The highest cooling enhancement ratio with a mist of 10% (weight) is about 20%. The relatively low cooling enhancement under GT operating conditions was also reported in [20], which revealed that the performance can be improved by employing different injection angles as well as blowing ratios. Note that cooling enhancement should be evaluated differently under different operating conditions when the absolute surface temperature reduction is important. For example, a 20% cooling effectiveness enhancement can result in a decent 180K reduction in wall temperature under elevated GT operating conditions.

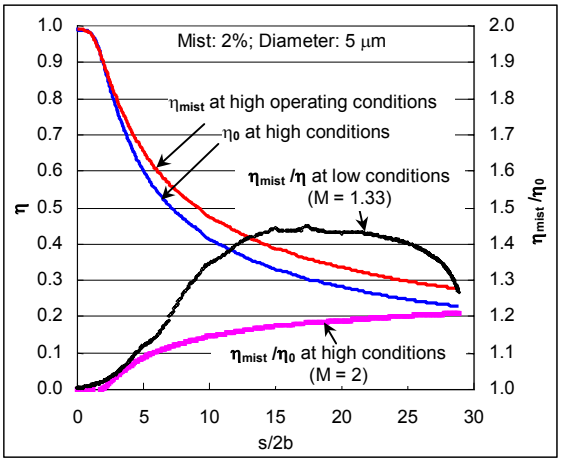

Figure 10 Effect of elevated operating conditions on mist film cooling performance of the turbine blade leading edge

2. Mist Film Cooling with Curvature Effect on Pressure and Suction Sides (2-D Slot)

2.1 Air-only Film Cooling on Pressure and Suction Sides

Since the flow fields over the curved surfaces are expected to create a body force exerted on the water droplet by the cross-stream pressure gradient, it is essential to examine the behavior of mist film cooling with the downstream curvature on both pressure and suction sides. To realize the effect of curvature on mist film cooling, the air film cooling is simulated first as a baseline for comparison. The injection angles for both sides are the same, 35°, and the injection momentums are also the same. Figure 11 shows that the suction side has a higher flow velocity (or cross-flow) than the pressure side, which results in a smaller effective blowing ratio in the suction side. A small recirculation (separation) region occurs in both sides immediately downstream of the injection hole. To optimize the mist film cooling performance, the injection velocity as well as the angle needs to be designed differently for these two sides.

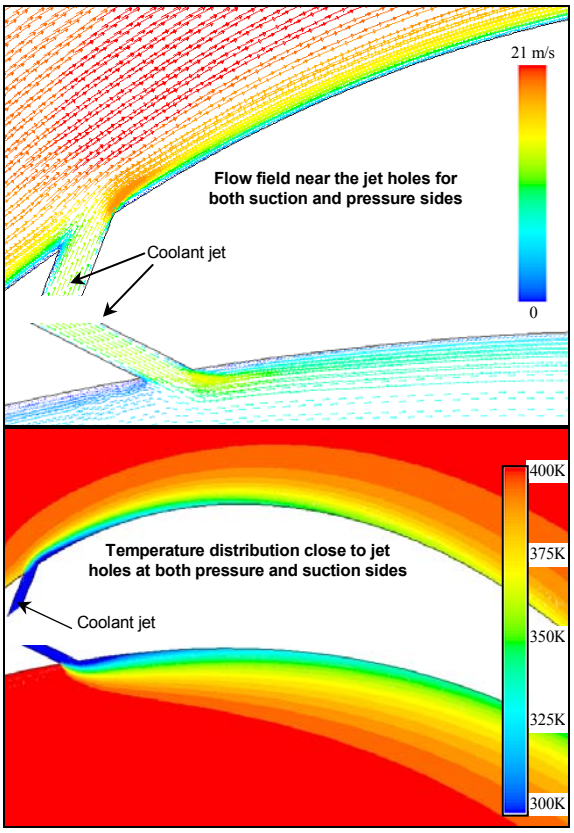

Figure 11 Flow pattern and temperature distribution of film cooling under the curvature effect on pressure and suction sides.

Figure 12 shows the adiabatic cooling effectiveness of air film cooling for both suction and pressure sides. The η values for both curved surfaces are lower than that over a flat surface but higher than the case at the leading edge. The poor performance at the leading edge is caused by the impingement of main flow against the injection coolant and less cross-flow near the leading edge to sweep the coolant jet downstream.

At the 2-D settings in this study, the pressure (concave) side shows a higher cooling effectiveness than the suction (convex) side. This is consistent with the results of Nicolas and Le Meur [11] and the high blowing ratio results of Schwarz et al. [14], but contrary to the results of Mayle et al. [12] and Berhe and Patankar [16]. When comparison is made between the flat surface and the curved surface, Mayle et al. [12] and Berhe and Patankar [16] reported that η values are higher on the convex surfaces than on the flat surfaces. So did Schwarz et al. [14] with low blowing ratio cases. The inconsistent results from previous studies [12-16] imply that the effect of curvature on film cooling is closely related to the geometrical settings (such as the hole configuration and injection angles) and flow parameters (such as the blowing ratio and main flow characteristics). The comparison will not be conclusive unless all the setting conditions are consistent. Irrespective of the inconsistency in the results of air-only film cooling on curved surfaces, the focus in this study is on investigating the potential cooling enhancement by injecting mist into the coolant. By using the current approach, the thermodynamic, heat transfer, and major flow characteristics of the mist flow are expected to be adequately simulated.

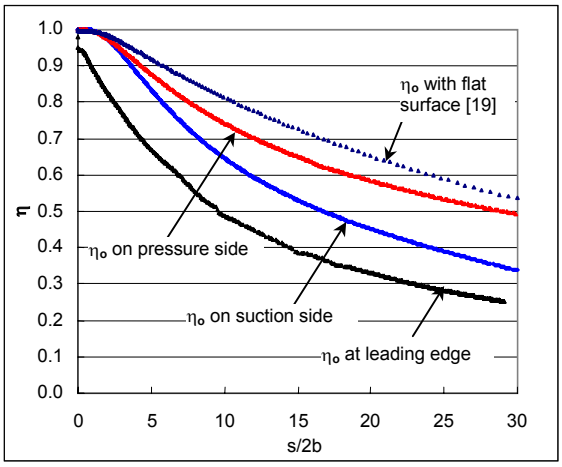

Figure 12 Comparison of air-only film cooling effectiveness on flat and curved surfaces with a nominal blowing ratio of 1.33.

2.2 Mist Enhancement on Film Cooling with Curved Surface

Figure 13 shows the cooling effectiveness of mist film cooling with curved surfaces. The mist concentration is 2%, and the droplet size is 5μm. The enhancement ratio on the pressure side is observed higher than on the suction side with the maximum enhancement of 61% on the pressure side and 31% on the suction side. It is believed that the difference in cooling enhancement is solely a consequence of the droplet thermal-fluid dynamics under the influence of curvature because the comparison reference is the air-only film cooling of each individual case.

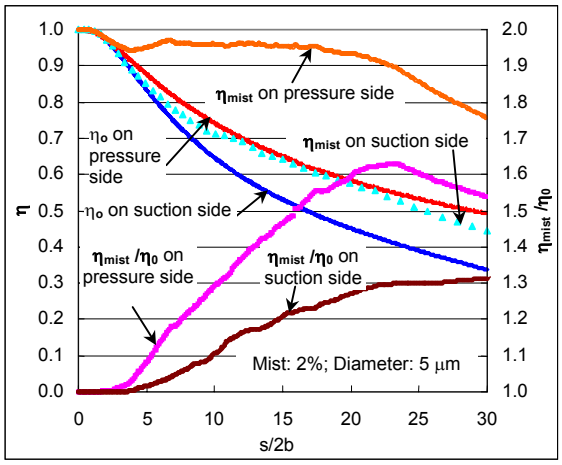

Figure 13 Enhancement of film cooling with mist injection on concave and convex surfaces.

To help investigate the droplet dynamics, the droplet trajectories are traced and given in Fig. 14. It is observed from this figure that the droplets in the convex side migrate away from the surface, and the droplets on the concave side tend to adhere closely to the wall. Other than the injection inertia, these phenomena can be simply explained as the centripetal force driving droplets away from the convex wall while the centrifugal force pushing droplets toward the concave wall. Hence mist-cooling enhancement is more pronounced on the pressure surface than on the suction surface. This seemingly easy explanation is

actually contrary to the boundary layer induced flow stability on the convex surface and instability on the concave surface.

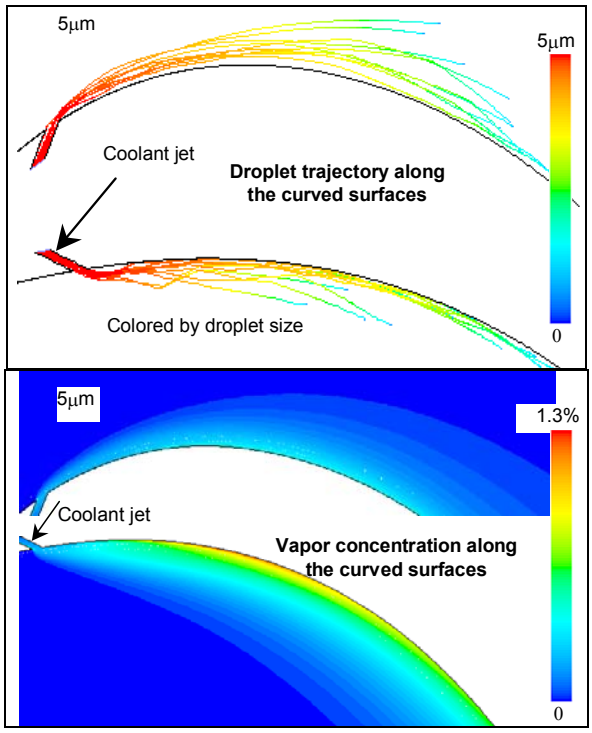

Figure 14 2-D droplet trajectories and vapor concentration in mist film cooling with concave and convex surfaces.

As early as 1917, Rayleigh [35] deduced the instability criterion for axisymmetical circular flow, which was later employed to explain "Streamwise convex curvature has a stabilizing effect on the boundary layer flow and concave curvature destabilizes the boundary layer flow." This statement would not be true if the flow was inviscid and no boundary layer would present. The inviscid flow theory gives a flow field with the velocity increasing with the radius away from the convex surface and decreasing with the radius away from the concave surface. The boundary layer actually disturbs this potential flow fields and presents a velocity deficit on both surfaces. This means that if the droplets were in the boundary layers, the droplets would migrate toward the convex wall and move away from the concave surface.

The contrary phenomenon shown in Fig. 14 can be explained as that the initial injection momentum of the coolant flow penetrates through the boundary layer and brings the droplets into the inviscid flow field. Therefore, the droplets are not subject to the instability of the boundary layer flow over the curved surfaces, rather, before they reach equilibrium the droplets are subjected to the local cross-stream pressure gradient that generates centrifugal body force over the concave side and centripetal force on the convex side. When the boundary layer grows thicker, some of the droplets were entrained into the boundary layer and move toward the convex surface further downstream on the convex surface as shown in Fig. 14. In a 3-D flow, the droplet dynamics can be further complicated by the secondary flows induced by the coolant jet. If the blowing ratio is different, the global phenomena could be changed and the film cooling effectiveness could be even reversed, but the fundamental mechanisms should be invariant. The droplet dynamics in Fig. 14 does not involve the complexity of the secondary flow because only 2-D flow filed is simulated.

The concentration of vapor due to droplet evaporation is also presented in Fig. 14. The concentration on the pressure side is higher than that on the suction side, which is consistent with the high cooling enhancement on the pressure side. The primary reason is the droplet dynamics discussed earlier and the low average velocity of the free stream close to the pressure surface.

3. Film Cooling of 3D Leading Edge

The results shown in Sections 1 and 2 are for the cases of two-dimensional slot jet. Although 2-D cases can be used to investigate the basic mechanism of mist film cooling under the influence of curvature, the real applications are usually 3-D with complicated injection geometries and flow parameters, which are subject to effects of end-wall and of rotation. To simplify the real applications, only a row of holes at the leading edge is considered. Furthermore, the effect of end walls is ignored, so the row of holes can be simplified as a single hole periodically appears in the radial direction from the hub to the tip. The distance between the periodic boundaries is 10 mm in the radial direction. The hole has a diameter of 1mm. The injection angle is 55^o to the main flow direction or 35^o to the surface tangent (see Fig. 1c). Figure 15 shows the temperature distribution on the blade surface. The surface temperature is low at the region immediate downstream of the cooling jet, and the cooling effect gradually becomes negligible. For the case shown in the figure, the jet primarily flows to the suction surface. Adjusting the incident angle or the cooling jet location can significantly change the areas covered by the cooling film. Multiple rows of cooling holes arrangement can mitigate the problems of changing loads or incident angles.

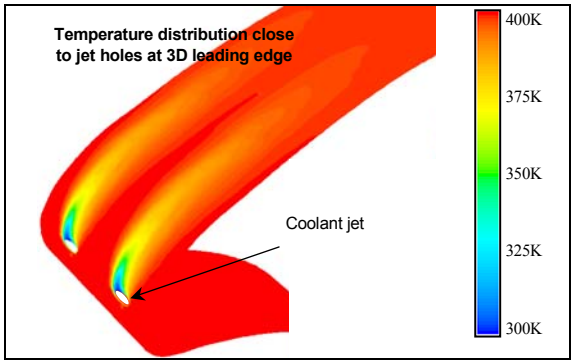

Figure 15 Temperature distribution of air film cooling on 3-D leading edge surface

Figure 16 shows the adiabatic film cooling effectiveness along the centerline of the injection hole in the 3-D domain. Compared to the 2-D case (see Fig. 4), the coolant coverage is weaker for the 3-D case due to the strong mixing and secondary flow folding between the jet and main flows. A peak value of η (0.9) is observed around s/d = 1.5 with relatively low cooling effectiveness (η<0.9) in the proximity of the injection hole (s/d<1.5). This is different from the monotonously decreasing η value shown in 2-D cases in Fig. 4. Figure 16 further indicates a sharp drop of η to a very low level within a short distance downstream. For instance, η drops to 20% at s/d = 8 and further down to 10% at s/b=12. With a 2% mist injection, the cooling effectiveness increases, although it is still low. The cooling enhancement is noticeable with the highest enhancement of 55% at s/d =25. Note that the jiggles on the curves are mostly caused by the numerical iteration

method used with the stochastic droplet tracking [19]. A solid line fairing through the jiggled points represents more realistic cooling enhancement values. The span-averaged value is also given in the figure. Although the span-averaged value is low, the mist enhancement is even more significant with a maximum level of 56%. At the same location (s/d), the average enhancement ratio is higher than that along the centerline.

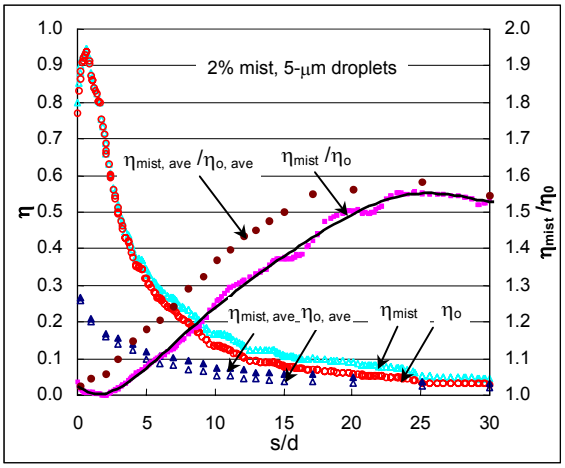

Figure 16 Adiabatic cooling effectiveness of 3D leading edge film cooling and its enhancement with mist injection

4. Validation of Simulation Results

It is important to verify any numerical solution with experimental data. However, there is not yet any experimental data available in the public literature for mist film cooling, either with simple or complicated geometries. The general methodology, modeling, and the numerical algorithm employed in this study are based on the validations established by authors in previous studies [18-19]. Before the simulated results are validated with experimental data, the results of this study can be fairly treated as qualitative descriptions of mist film cooling performance under the effects of various studied parameters.

CONCLUSIONS

This paper studies the mist film cooling effectiveness near the leading edge of a turbine blade and on the blade surfaces subject to curvature (concave and convex) effect. Numerical simulation is employed with different settings and operating parameters. In general, injection of mist into the coolant flow can increase the adiabatic film cooling effectiveness (η) at the leading edge and on the curved side walls. Smaller droplets achieve better cooling enhancement. The major findings are:

- In the 2-D settings of this study, air-only adiabatic film cooling effectiveness (η) degrades under the effect of curvature in the following descending order: flat surface > concave (pressure) surface > convex (suction) surface > leading edge. These results are consistent with some published studies while inconsistent with others due to the sensitivity of the results to the different parameters such as blowing ratio, injection angle, and strength of the curvature.

- The leading edge film cooling can be significantly affected by changing of the incident angle due to startup or part load operations. The film cooling coverage could switch from the suction side to the pressure side and leaves the surface of the other part unprotected by the cooling film.

- 2-D mist film cooling achieves higher enhancement on the pressure side than on the suction side. The maximum mist cooling enhancement is approximately 60% on the pressure side and 30% on the suction side.

- The water droplets traces show the centrifugal force pushes droplets toward the concave wall and the centripetal force drives droplets away from the convex wall, hence mist cooling enhancement is more pronounced on the pressure surface than on the suction surface. This observation is contrary to the boundary layer induced flow stability on the convex surface and instability on the concave surface. A hypothetical explanation is given as that most of the droplets are outside the boundary layer after being injected into the main stream and before they reach equilibrium with the local pressure field, the local cross-stream pressure gradient generates centrifugal body force over the concave side and centripetal force on the convex side.

- 3-D simulation of the leading edge film cooling shows along the centerline a relatively low η near the hole and a peak η at s/d=1.5. Adding 2% mist (weight) can achieve an average of 30% cooling enhancement with the highest local enhancement reaching 55% at s/d =25. Although the span-average cooling effectiveness is low, the mist enhancement is higher than that along the centerline.

- Under real gas turbine operating conditions at high pressure, temperature, and velocity, the enhancement of mist cooling achieves 20%, which seems lower than under low T-P-V condition. However, a decent wall cooling of 180K can be achieved by 20% enhancement in contrast to 50K wall temperature reduction with 50% cooling enhancement under low T-P-V conditions.

ACKNOWLEDGEMENT

This study is partially supported by the Louisiana Governor's Energy Initiative via the Clean Power and Energy Research Consortium (CPERC) and administrated by the Louisiana Board of Regents.

REFERENCES

[1] Eriksen, V.L. and Goldstein, R. J., 1974, "Heat Transfer and Film Cooling Following Injection Through Inclined Tubes," ASME J. Heat Transfer, **96**, pp. 239–245.

[2] Goldstein, R. J., Eckert, E. R. G., and Burggraf, F., 1974, "Effects of Hole Geometry and Density on Three-Dimensional Film Cooling," Int. J. Heat Mass Transfer, **17**, pp. 595–607.

[3] Jia, R., Sunden, B., Miron, P., and Leger, B., 2003, "Numerical and Experimental Study of the Slot Film Cooling Jet with Various Angles," Proceedings of the ASME Summer Heat Transfer Conference, pp. 845-856.

[4] Kwak, J. S. and Han, J. C., 2003, "Heat Transfer Coefficients and Film-Cooling Effectiveness on a Gas Turbine Blade Tip," ASME J. Heat Transfer, **125,** pp. 494-502.

[5] Kwak, J. S. and Han, J. C., 2003, "Heat transfer Coefficients and Film Cooling Effectiveness on the Squealer Tip of a Gas Turbine Blade," ASME J. Turbomachinery, **125**, pp. 648-657.
[6] Wang, T., Chintalapati, S., Bunker, R. S., and Lee, C. P., 2000, "Jet Mixing in a Slot," Experimental Thermal and Fluid Science, **22**, pp. 1-17.
[7] Bell, C. M., Hamakawa1, H., and Ligrani, P. M., 2000, "Film Cooling From Shaped Holes," ASME J. Heat Transfer, **122,** pp. 224-232.
[8] Brittingham, R.A. and Leylek, J. H, 2002, "A Detailed Analysis of Film Cooling Physics: Part IV—Compound-Angle Injection with Shaped Holes," ASME J. Turbomachinery, **122,** pp. 133-145.
[9] Colban, W., Thole, K. A., and Haendler, M., 2006, "A Comparison of Cylindrical and Fan-shaped Film Cooling on a Vane Endwall at Low and High Free Stream Turbulence Levels," ASME Turbo Expo 2006*,* Paper No 2006-90021.
[10] Suryanarayanan, A., Mhetras, S. P., Schobeiri, M. T., and Han, J. C., 2006, "Film-cooling Effectiveness on a Rotating Blade Platform," ASME Turbo Expo 2006*,* Paper No 2006-90034.
[11] Nicolas, J. and Le Meur, A., 1974, "Curvature Effects on Turbine Blade Cooling Film," ASME paper, No 74-GT-156.
[12] Mayle, R. E., Kopper, F. C., Blair, M. F., and Bailey, D. A., 1977, "Effect of Streamline Curvature on Film Cooling," ASME J. of Engineering for Power, **99,** Ser A, pp. 77-82
[13] Ito, S., Goldstein, R. J., and Eckert, E. R. G., 1978, "Film Cooling of a Gas Turbine Blade," ASME J. Eng. Power, **100**, pp. 476–481.
[14] Schwarz, S.G., Goldstein, R.J. and Eckert, E.R.G., 1991, "Influence of Curvature on Film Cooling Performance," ASME J. of Turbomachinery, **113**, pp. 472-478.
[15] Jiang, H. W. and Han, J.-C, 1996, "Effect of Film Hole Row Location on Film Effectiveness on a Gas Turbine Blade," ASME J. of Heat Transfer, **118**, pp. 327-333
[16] Berhe, M.K. and Patankar, S.V, 1999, "Curvature Effects on Discrete-hole Film Cooling," ASME J. of Turbomachinery, **121**, pp. 781-791.
[17] Kim, K.-S., Kim, Y. J., and Kim, S.-M., 2006, "Enhancement of Film Cooling Performance at the Leading Edge of Turbine Blade," ASME Turbo Expo 2006*,* Paper No 2006-90321.
[18] Li, X. and Wang, T., 2005, "Simulation of Film Cooling Enhancement with Mist Injection," ASME Journal of Heat Transfer, **128**, pp. 509-519.
[19] Li, X. and Wang, T., 2005, "Effects of Various Modeling on Mist Film Cooling," Proc. ASME Int. Mechanical Engineering Congress and Exhibition (IMECE 2005-81780), Orlando, Florida, November 2005.
[20] Wang, T. and Li, X., 2006, "Simulation of Mist Film Cooling at Gas Turbine Operating Conditions," ASME Turbo Expo 2006, Barcelona, Spain, May 8-11.
[21] Li, X. and Wang, T., 2006, "Two-phase Flow Simulation of Mist Film Cooling with Different Wall Heating Conditions," 13th International Heat Transfer Conference, Sydney, Australia, 06.
[22] Chaker, M., Meher-Homji, C.B., and Mee, M., 2002, "Inlet Fogging of Gas Turbine Engines - Part A: Fog Droplet Thermodynamics, Heat Transfer and Practical Considerations," ASME Proceedings of Turbo Expo 2002*,* **4**, pp. 413-428.
[23] Petr, V., 2003, "Analysis of Wet Compression in GT's," Energy and the Environment - Procs of the International Conference on Energy and the Environment, **1**, pp. 489-494.
[24] Nirmalan, N.V., Weaver, J.A. and Hylton, L.D., 1998, "An Experimental Study of Turbine Vane Heat Transfer with Water-Air Cooling," J. of Turbomachinery, 120, No.1, pp.50-62.
[25] Guo, T., Wang, T., and Gaddis, J. L., 2000, "Mist/Steam Cooling in a Heated Horizontal Tube, Part 1: Experimental System, Part 2: Results and Modeling," ASME J. Turbomachinery, **122**, pp. 360–374.
[26] Guo, T., Wang, T., and Gaddis, J.L., 2001, "Mist/Steam Cooling in a 180^{o} Tube Bend," ASME J. Heat Transfer, **122,** pp. 749-756.
[27] Li, X., Gaddis, J. L., and Wang, T., 2003, "Mist/Steam Cooling by a Row of Impinging Jets," Int. J. Heat Mass Transfer, **46**, pp. 2279-2290.
[28] Li, X., Gaddis, J. L., and Wang, T, 2003, "Mist/Steam Heat Transfer with Jet Impingement onto a Concave Surface," ASME J. Heat Transfer, **125**, pp. 438-446
[29] Wang, M. J. and Mayinger, F., 1995, "Post-dryout Dispersed Flow in Circular Bends," Int. J. Multiphase Flow, **21**, pp. 437-454.
[30] Aggarwal, S.K. and Park, T.W., 1999, "Dispersion of Evaporating Droplets in a Swirling Axisymmetric Jet," AIAA Journal, **37**, pp. 1578-1587.
[31] Chen, X.-Q. and Pereira, J.C.F., 1995, "Prediction of Evaporating Spray in Anisotropically Turbulent Gas Flow," Numerical Heat Transfer; Part A: Applications, **27**, pp. 143-162.
[32] Wolfstein, M., 1969, "The Velocity and Temperature Distribution of One-Dimensional Flow with Turbulence Augmentation and Pressure Gradient," Int. J. Heat Mass Transfer, **12,** pp. 301-318.
[33] Launder, B. E. and Spalding, D. B., 1972, Lectures in Mathematical Models of Turbulence*,* Academic Press, London, England.
[34] Fluent Manual, Version 6.2.16, 2005, Fluent, Inc.
[35] Rayleigh, J.W. S., 1917, "On the Dynamics of Revolving Fluids," Proceedings of the Royal Society of London, **93**, Serial A, pp. 148-154.